# Volumetric Performance Evaluation of a Laser Scanner Based on Geometric Error Model

B. Muralikrishnan[1], M. Ferrucci[1], D. Sawyer[1], G. Gerner[2], V. Lee[1], C. Blackburn[1], S. Phillips[1], P. Petrov[3], Y. Yakovlev[3], A. Astrelin[3], S. Milligan[3], and J. Palmateer[4]

[1]National Institute of Standards and Technology, Gaithersburg, MD
[2]The Pennsylvania State University, Erie, PA
[3]Basis Software Inc., Redmond, WA
[4]Boeing Research and Technology, Seattle, WA

## Abstract

We discuss a geometric error model for those large volume laser scanners that have the laser source and a spinning prism mirror mounted on a platform that can rotate about the vertical axis. We describe the terms that constitute the model, address their effect on measured range and angles, and discuss the sensitivity of different two-face and volumetric length tests to each term in the model. We report on experiments performed using commercially available contrast targets to assess the validity of the proposed model. Geometric error models are important not only in improving the accuracy of laser scanners, but also in facilitating the identification of test procedures for performance evaluation of these instruments and therefore in the development of documentary Standards. The work described in this paper lays the foundation for such efforts.

## 1. Introduction

Large volume laser scanners are used for a variety of purposes including dimensional metrology of large artifacts, digitization and reverse engineering, historical preservation and archiving, etc. The extremely high data collection rates and noncontact measurements made possible through advancements in optoelectronics are rapidly shifting dimensional metrology toward this form of measurement. There are currently two broad mechanical designs of large volume laser scanners suitable for dimensional metrology. One design is similar in construction to a laser tracker, where the laser source is stationary and located in the base and the spinning mirror is mounted on the gimbal head. Such a design has already been discussed in the literature [1] and is not the focus of this paper.

In this paper, we present a geometric error model for the second design, which comprises those laser scanners that incorporate a source and a spinning mirror on a platform that can rotate about the vertical axis. We describe the terms in the model and their influence on the measured range and angles. The model parameters apply to front-face measurements of the scanner (vertical angle in the range of 0° to 180°) but some scanners, such as the one tested, also allow measurements in back face. That is, the target can be measured by rotating the scanner 180° about the vertical axis (i.e., the horizontal angle changes by 180°) and then rotating the mirror past 180° in the vertical angle to locate the target. We describe how corrections to the measured range and angles can be obtained for measurements made using both faces of the scanner. The model applies to all scanners that employ such a stacked construction and is not limited by the technology employed to detect range. The particular scanner considered in this study is a phase shift scanner that uses amplitude modulation to detect range [2].

The objective of this work is not simply to model errors for the purpose of reducing or eliminating their effects, but also to understand how these errors manifest as two-face or point-to-point length errors so that we may then identify suitable artifact test positions and orientations for the performance evaluation of these instruments. We therefore discuss possible placement of targets and reference lengths to achieve high sensitivity to the different terms in the model. We report on experiments performed using commercially available contrast targets to assess the validity of the proposed model.

Laser scanner measurements suffer from several other error sources such as those associated with the optical interaction of the laser and the part surface, the choice of targets, material properties, surface finish, reflectivity, etc. Determining the optimal positioning of targets and reference lengths to detect opto-mechanical scanner errors will comprise one test among a suite of performance tests for laser scanners. In this paper we only focus on the opto-mechanical errors of scanner performance evaluation and use target materials that minimize the interaction of the scanner beam with the target properties.

It should be pointed out that most commercial laser scanner systems *do* incorporate a geometric error model within the system but that information is often proprietary. Further, scanner manufacturers may not necessarily provide the user with the ability to determine the parameters of the model (a procedure referred to as 'compensation') in-situ in a manner similar to that of laser trackers. This is possibly because laser scanner systems available today have less stringent accuracy specifications due to ranging errors that are substantially larger than errors induced by optical and geometric misalignments within the system. However, ranging accuracies of laser scanners have been improving steadily over the years and it will only be a matter of time before ranging errors are substantially smaller and scanner compensation will become an important aspect in performing accurate measurements. As in the case of laser trackers, ranging performance evaluation of a laser scanner along the radial direction can be done independently of volumetric performance evaluation. The focus of this paper is on evaluating the volumetric performance, not ranging.

Much of the focus of reported research [3-6] in the literature on scanner modeling is on the subject of self-calibration, that is, the development of procedures to mitigate the effects of geometric misalignments. The work described in this paper not only details the geometric misalignments within the system, but more importantly, suggests placement of targets and reference lengths in order to expose the presence of such errors, thus facilitating the creation of documentary (national or international) Standards for performance evaluation in the future.

## 2. Coordinate system and terminology

First we define the coordinate system associated with a perfect laser scanner. In later sections we will address the geometric errors in the scanner. Consider a Cartesian coordinate system *XYZ* that is fixed to the scanner base with its origin located at *O* as shown in Fig. 1. The *Z* axis is referred to as the vertical axis or the standing axis and the *XY* plane is referred to as the horizontal plane. We define the Z axis to be coincident with the vertical rotation axis of the scanner. The mirror rotation axis is referred to as the horizontal axis, also known as the transit axis. Two axes *OT* and *ON* are attached to the platform which rotates about the *Z* axis. Axis *OT*

is defined to be coincident with the horizontal axis of a perfect scanner and is defined to be in the *XY* plane. Point *O* is also the point where the laser strikes the mirror (for a perfect scanner) and is reflected towards the target *P*. Axis *ON* is normal to *OT* and also lies on the *XY* plane and is oriented such that *ON, OT,* and *OZ* form a right handed coordinate system. Point *O*' lies on the *OT* axis and is the source where the laser is emitted. After reflection off the mirror the laser beam path lies in the *ONZ* plane, this also defines the normal to the mirror surface to be tilted at a 45 degree angle with respect to axis *O'T*. We refer to the plane *O'OP* as the laser plane; this plane contains the laser beam emitted from the source and the beam reflected to the target *P*. Axes *O'N'* and *O'Z'* intersect at point *O*' and are parallel to *ON* and *OZ,* respectively.

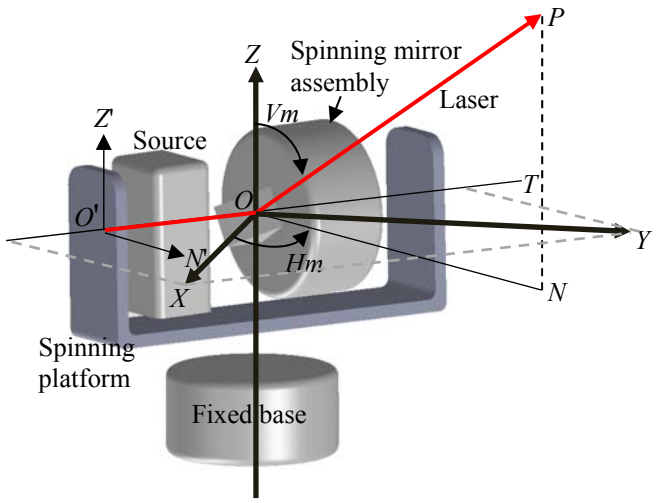


**Figure 1** *Coordinate system definition for a perfect scanner*

We adopt the following terminology. The measured range, horizontal angle, and vertical angle are denoted by *Rm*, *Hm*, and *Vm* respectively. The corrected range and angles are denoted by *Rc*, *Hc*, and *Vc* respectively. The corrections to the range and angles are denoted by $\Delta Rm$, $\Delta Hm$, and $\Delta Vm$. For the purposes of computing errors associated with geometric misalignments in the scanner, the corrected values are also assumed to be the true values; we do not consider random errors in this paper. The corrections are added to the measured values to obtain a better estimate of the corresponding quantities. The corrections have the opposite sign than their associated error and hence the corrections are the differences between the true values and the measured values.

The directions for the positive (increasing) horizontal and vertical angles are shown in Fig. 1. The horizontal angle *Hm* is the extent of the angular rotation of the spinning platform about the vertical axis. The Vertical angle *Vm* is the extent of rotation of the spinning mirror about the horizontal axis. While the pole (+*Z* axis) is the zero for vertical angle measurements, there is no absolute zero for horizontal angle measurements for the scanner that we tested. The spinning platform can be positioned at any orientation and set as the zero.

## 3. Model parameters

There are several sources of offsets, tilts, and eccentricities in the opto-mechanical construction of the laser scanner that may produce errors in the measured coordinates. We describe them in this section; a list is provided in Table 1. The equations presented in this paper are simply stated but can be derived using simple trigonometry. They are valid to first order in $x/R$, where $x$ is the offset and $R$ is the range value, over the entire measurement volume except for the points near the poles, *i.e.,* $Vm = 0°$ and $Vm = 180°$. The $Vm = 180°$ case is unimportant since the scanner tripod blocks this region from being measured. The region near the pole (e.g., within 1°) where $Vm = 0°$ is more complicated. In particular, several of the error correction terms have singularities at the poles. Additionally, some error sources such as mirror offset (section 3.3) prevent the scanner from physically directing the laser beam in the pole (i.e., Z) direction even though the scanner will report measured values with $Vm = 0°$. Consequently, it is recommended that measurement data with $Vm$ near zero be rejected because the uncorrected data is unreliable and the corrections are not applicable. A more complex model that accounts for these effects will be addressed in another publication.

**Table 1: Model parameters for the scanner**

| Parameter | Description | Two-face sensitivity | Sensitive length tests[1] | Correction terms[2] |
|---|---|---|---|---|
| $x_{1n}$ | Beam offset along $n$ | Vertical angle direction | Asymmetrical horizontal length test | $\Delta Hm_1$, $\Delta Vm_1$ |
| $x_{1z}$ | Beam offset along $z$ | Horizontal angle direction | Asymmetrical vertical length test | $\Delta Hm_2$, $\Delta Vm_2$ |
| $x_2$ | Transit offset | Vertical angle and ranging direction | Scanner placed in line and in between two targets | $\Delta Rm_1$, $\Delta Vm_3$ |
| $x_3$ | Mirror offset | Horizontal angle direction | Asymmetrical horizontal length test | $\Delta Rm_3$, $\Delta Hm_3$ |
| $x_4$ | Vertical index offset | Vertical angle direction | Symmetrical horizontal length test with the length positioned at an elevation | $\Delta Vm_4$ |
| $x_{5n}$ | Beam tilt component along $n$ | Vertical angle direction | Symmetrical vertical length test | $\Delta Hm_4$, $\Delta Vm_5$ |
| $x_{5z}$ | Beam tilt component along $z$ | Horizontal angle direction | Symmetrical left and right diagonal test | $\Delta Hm_5$, $\Delta Vm_6$ |
| $x_6$ | Mirror tilt | Horizontal angle direction | Asymmetrical diagonal test | $\Delta Hm_6$ |
| $x_7$ | Transit tilt | Horizontal angle direction | Symmetrical left and right diagonal test | $\Delta Hm_7$ |
| $x_{8x}$ | Horizontal angle encoder eccentricity component along $x$ | Horizontal angle direction | Symmetrical horizontal length test | $\Delta Hm_8$ |
| $x_{8y}$ | Horizontal angle encoder eccentricity component along $y$ | Horizontal angle direction | Symmetrical horizontal length test | $\Delta Hm_9$ |
| $x_{9n}$ | Vertical angle encoder eccentricity component along $n$ | Vertical angle direction | Symmetrical vertical length test | $\Delta Vm_7$ |
| $x_{9z}$ | Vertical angle encoder eccentricity component along $z$ | | Symmetrical horizontal length test with the length positioned at an elevation | $\Delta Vm_8$ |
| $x_{10}$ | Zero-offset (Bird-bath error) | | Scanner placed in line and in between two targets | $\Delta Rm_3$ |
| $x_{11a}$ | Second order scale error in the horizontal angle encoder | | Long symmetrical horizontal length test far away from scanner | $\Delta Hm_{10}$ |
| $x_{11b}$ | Second order scale error in the horizontal angle encoder | | Long symmetrical horizontal length test far away from scanner | $\Delta Hm_{11}$ |
| $x_{12a}$ | Second order scale error in the vertical angle encoder | | Asymetrical diagonal length test | $\Delta Vm_9$ |
| $x_{12b}$ | Second order scale error in the vertical angle encoder | | Symmetrical vertical length test | $\Delta Vm_{10}$ |

[1]There may be many positions and orientations of a reference length that are sensitive to any given term in the model. We only list one illustrative position here.
[2]The correction terms are described in subsequent sections

### 3.1 Beam offset ($x_{1n}$ and $x_{1z}$)

*Description*: We are interested in obtaining the true values of the coordinates to a target at point $P$. Suppose the laser beam strikes the mirror at a point $O_1$ that is offset by $x_1$ from its ideal location $O$ as shown in Fig. 2. This could arise, for example, by the laser source being displaced

from its ideal position $O'$ by a constant offset ($x_1$) to emerge from $A_1$, as shown in Fig. 2. An offset beam can also arise in combination with a beam originating from $O'$ having a beam tilt error and thus striking the mirror at $O_1$; beam tilt errors will be addressed in section 3.5. In this section we address a pure beam offset and hence the beam is parallel to the $OT$ axis. The offset beam strikes the mirror at $O_1$ and travels along the $O_1P_1$ direction. A perfect scanner would have measured the target $P$ and recorded the correct coordinates as shown in Fig. 2. At another time the beam is directed to the point $P$, and the horizontal and/or vertical angles have different values than when the beam was directed along the $O_1P_1$ direction. The magnitude of the corrections to these measured angles can be estimated by resolving the beam offset into two components, $x_{1n}$ along the $ON$ direction, and $x_{1z}$ along the $OZ$ direction. Each component produces an error in both the measured horizontal and vertical angles. From the geometry shown in Fig. 2, the corrections to the measured front-face angle can be derived as

$$\Delta Hm_1 = (x_{1n} \sin Vm)/(Rm \sin Vm) = x_{1n}/Rm \quad (1)$$

$$\Delta Hm_2 = (x_{1z} \cos Vm)/(Rm \sin Vm) = x_{1z}/(Rm \tan Vm)$$

$$\Delta Vm_1 = (x_{1n} \cos Vm)/Rm$$

$$\Delta Vm_2 = (-x_{1z} \sin Vm)/Rm,$$

where $Rm$ is the measured range. The subscript $i$ in $\Delta Hm_i$ and $\Delta Vm_i$ is simply an index that will be used for summing over all the component corrections arising from each term in the model in order to obtain the total correction for the vertical, horizontal, and range values.

*Two-face tests*: Laser scanners typically have the capability to measure a point in both front-face and back-face. In back-face the scanner has changed the horizontal angle by 180° and the vertical angle has continued to increase until the laser beam of a perfect scanner points at the same nominal point as it did in the front-face measurement. It should be noted that $x_{1z}$ is sensitive to two-face testing along the horizontal angle direction but not along the vertical angle direction, while the reverse is true for $x_{1n}$. Therefore $\Delta Hm_2$ and $\Delta Vm_1$ reverse in sign in the back-face but $\Delta Hm_1$ and $\Delta Vm_2$ do not. Two-face sensitivity arises from the geometry of the construction, not from the functional form of the equations. The two-face error $E$ is defined as the distance (always a positive quantity) between the coordinate measured in front-face and the coordinate measured in back-face of the same target [7]. For $x_{1n}$, this is given by

$$E = 2(\Delta Vm_1)Rm = 2|x_{1n} \cos Vm| \quad (2)$$

and for $x_{1z}$, this is given by

$$E = 2(\Delta Hm_2)Rm \sin Vm = 2|x_{1z} \cos Vm|. \quad (3)$$

Higher sensitivity is obtained for both terms when the target is placed near the pole or on the floor, there being no dependence on the range to the target.

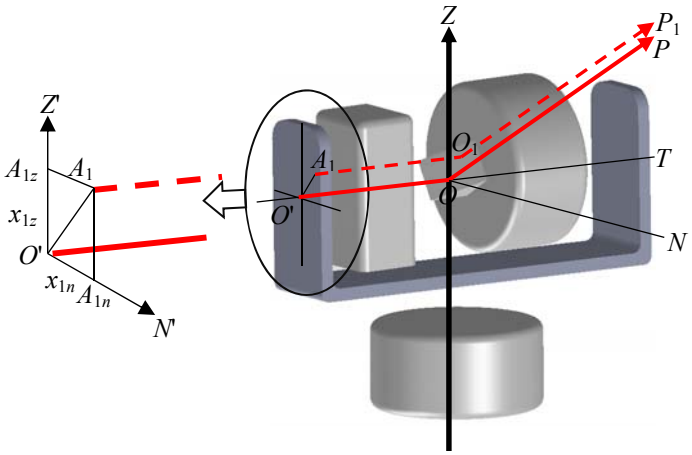


**Figure 2** *Geometry of beam offsets in the front face. The offset beam originates from $A_1$, strikes the mirror at $O_1$, and travels to $P_1$ instead of P. In order to direct the beam to the target P, the horizontal and/or vertical angle axes have to be exercised, which results in horizontal and/or vertical angle readings being different from the true values.*

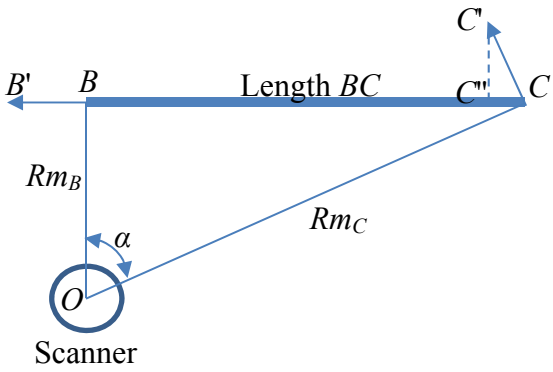


$BB' = Rm_B\,(x_{1n}/\,Rm_B) = x_{1n}$
$CC' = Rm_C\,(x_{1n}/\,Rm_C) = x_{1n}$
$CC'' = x_{1n}\cos\alpha$
Length error = $BB' - CC'' = x_{1n}(1-\cos\alpha)$

**Figure 3** *Sensitivity of the asymmetrical horizontal length test to $x_{1n}$ shown in the figure (top view).*

*Volumetric length tests*: As mentioned in [8], sensitivity of a model parameter to a length test is achieved if the error vectors at the two ends of the length have components along the length with a non-zero sum. Each offset term produces errors in both the horizontal and the vertical angle. Therefore, there will be numerous possible positions and orientations of a reference length that satisfy the aforementioned condition. An example of a length test that is sensitive to $x_{1n}$ is shown in Fig. 3 (top view shown). In that figure, the scanner is placed close to one end of a horizontal length *BC* instead of at the center. We refer to this position as the asymmetrical horizontal length test. The offset $x_{1n}$ produces horizontal angle errors at *B* and *C* resulting in measured coordinates being located at *B'* and *C'*. The components of these errors along the direction of the length are *BB'* and *CC''*. Even though these components are along the same direction, they are not of equal

magnitude. The resulting sum is non-zero as shown in Fig. 3. An asymmetric vertical length is sensitive to $x_{1z}$ for a similar reason. It should be noted that these are not the only sensitive positions for these terms. An example of another sensitive position for both terms is a symmetrical horizontal length test (scanner placed centrally with respect to both ends) with the length positioned at an elevation (not at scanner height).

### 3.2 **Transit offset ($x_2$)**

*Description*: If the horizontal (mirror rotation) axis and the laser beam axis are coincident but shifted together so that they do not intersect the vertical axis at *O*, this offset can be resolved into two components, one along *OZ* and the other along *ON*. The component along the *OZ* direction is not of any consequence as it is equivalent to a translation of the origin *O* along the *Z* axis. The component along the *ON* direction will produce an error in the range and vertical angle readings. (For the case where the mirror rotation axis shifts a different amount than the laser beam, this can be considered as a combination of shifting them both together, followed by a beam offset (*i.e.,* $x_{1n}$ ) described in section 3.1.)

Consider a shift in the mirror rotation and laser beam axis along the *ON* direction by an amount $x_2$ (taken as positive when in the *+N* direction) to point $O_2$ as shown in Fig. 4(a); the horizontal axis now passes through $O_2$ and into the plane of the paper. The path of the ideal beam from *O* to target *P* is shown in the figure along with the path of the actual beam from $O_2$ to target $P_2$ due to the transit offset. But in order to direct the offset beam to the target, the spinning mirror has to rotate counterclockwise by an angle $(x_2\cos Vm)/Rm$. The measured vertical angle will therefore be smaller than the true angle. The correction is given by

$$\Delta Vm_3 = (x_2\cos Vm)/Rm. \quad (4)$$

The measured range will also be smaller than the true range; the correction to the range is given by

$$\Delta Rm_1 = x_2\sin Vm. \quad (5)$$

*Two-face tests***:** Transit offset is sensitive to two-face testing along both the ranging and vertical angle directions. The two-face error *E* along the vertical angle direction is given by

$$E = 2(\Delta Vm_3)Rm = 2|x_2\cos Vm|. \quad (6)$$

Highest sensitivity is obtained by placing a target near the pole or on the floor where $\cos Vm$ is a maximum; while there is no range dependence at all, in order to maximize $\cos Vm$ the target is usually required to be close to the scanner. The two-face error *E* along the ranging direction is given by

$$E = 2(\Delta Rm_1) = 2|x_2\sin Vm|. \quad (7)$$

Highest sensitivity is obtained by placing a target at scanner height where $\sin Vm = 1$. In both these two-face error calculations either the front–face or back-face *V*m value may be used and although they are different the change to the *E* value is much less than one part in a thousand.

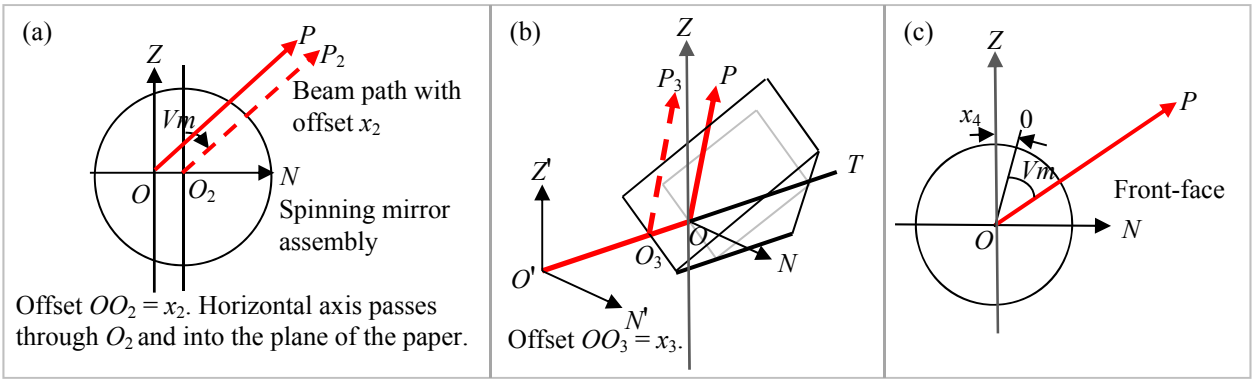


**Figure 4** (a) *Transit offset* (b) *Mirror offset* (c) *Vertical index offset*

*Volumetric length tests*: The transit offset is sensitive to a length test where the scanner is placed in-line and in-between two targets (at scanner height), where the distance between targets has already been calibrated by other means.

### 3.3 **Mirror offset ($x_3$)**

*Description*: In the ideal case, the plane of the mirror intersects the horizontal axis and the vertical axis at point $O$. If that plane is offset from its ideal location along axis $O'T$ (with a positive displacement defined in the $OT$ direction) by an amount $x_3$ then the laser beam strikes the mirror at a point $O_3$ (as shown in Fig. 4(b) for the case where $x_3$ is negative) and travels to $P_3$. The distance the laser beam travels to $O_3$ is the distance $O'O + x_3$; in Fig 4(b) $x_3$ is negative and consequently the path to the mirror is foreshortened. The scanner will hence make a range error of $x_3$ and thus the correction that must be added to the measured range value is $-x_3$ and denoted

$$\Delta Rm_2 = -x_3. \quad (8)$$

The reflection from point $O_3$ also results in an angular error (i.e., the measured horizontal angle minus the horizontal angle of point $P_3$) of $-x_3/(Rm \sin Vm)$. The correction to the horizontal angle is therefore given by

$$\Delta Hm_3 = x_3/(Rm \sin Vm). \quad (9)$$

In some scanner systems there is a reference surface located below the mirror in the $Vm = 180°$ direction that is used to set $Rm = 0$ at point $O_3$ and thus compensate for the ranging effects of the $x_3$ displacement. Using this technique, $\Delta Rm_2 = 0$ but the angular error still persists, and so the corresponding compensation value $\Delta Hm_3$ is still required. The data collected and described later in this paper uses a scanner that employs such a reference surface and consequently we omit the $\Delta Rm_2$ correction term during its analysis.

*Two-face tests*: Mirror offset is sensitive to two-face testing along the horizontal angle direction; the ranging error does not change and hence is insensitive to the reversal. The two-face error $E$ is given by

$$E = |2(\Delta Hm_3) Rm \sin Vm| = 2|x_3|. \quad (10)$$

The sensitivity is constant at any point in the work volume and is equal to twice the offset.

*Volumetric length tests*: The asymmetric horizontal length test (shown in Fig. 3) is one example of a length test that is sensitive to this term.

### 3.4 Vertical index offset ($x_4$)

*Description*: A shift in the zero of the vertical angle encoder from the *Z* direction results in a constant error in the measured vertical angle, a misalignment parameter referred to as vertical index offset and denoted $x_4$. A positive vertical index shift is in the $+V$ direction as shown in Fig. 4(c). The error in the front-face vertical angle is $Vm$ (the measured vertical angle) minus the vertical angle of point *P* from the pole and is $-x_4$, i.e., a negative value as shown in Fig 4 (c). The correction to the vertical angle is therefore given by

$$\Delta Vm_4 = x_4. \tag{11}$$

*Two-face tests*: Vertical index offset is sensitive to two-face testing along the vertical angle direction. The two-face error *E* is given by

$$E = |2(\Delta Vm_4)Rm| = 2Rm|x_4|. \tag{12}$$

The two-face error is larger when the target is farther away from the scanner.

*Volumetric length tests*: A symmetrical horizontal length test (scanner placed centrally with respect to both ends) with the length positioned as close to the scanner as possible (so that the change in horizontal angle is as large as possible) and at an elevation as high as possible (so that the vertical angle is small) will result in the error vectors at each end of the length to either point towards each other or away from each other resulting in high sensitivity to this term.

### 3.5 Beam tilt ($x_{5n}$ and $x_{5z}$)

*Description*: In addition to an offset, the laser emerging from the source may also suffer from a tilt error meaning that the beam is not parallel to the *OT* axis. Fig. 5 shows a pure beam tilt error with the laser emerging from point $A_5$ to strike the mirror at point *O*. (If the beam does not strike the mirror at *O*, that effect is modeled by the beam offset term described in section 3.1). The tilt in the laser can be resolved into two components $x_{5n}$ and $x_{5z}$ as shown in Fig. 5. The beam tilt is expressed in units of angle, i.e., $x_5/OO'$. For positive offsets, as shown in Fig. 5, the corrections are given by

$$\Delta Hm_4 = (x_{5n}\sin Vm)/\sin Vm = x_{5n} \tag{13}$$
$$\Delta Hm_5 = (x_{5z}\cos Vm)/\sin Vm = x_{5z}/\tan Vm$$
$$\Delta Vm_5 = x_{5n}\cos Vm$$
$$\Delta Vm_6 = -x_{5z}\sin Vm.$$

*Two-face tests*: Both tilt components are sensitive to two-face testing. As in the case of beam offset, $\Delta Hm_5$ and $\Delta Vm_5$ reverse in sign in back-face, but $\Delta Hm_4$ and $\Delta Vm_6$ do not. The two-face error *E* for $x_{5n}$ is given by

$$E = 2\,Rm\,|(\Delta Vm_5)\,| = 2Rm|x_{5n}\cos Vm| \tag{14}$$

and that for $x_{5z}$ is given by

$$E = 2Rm|(\Delta Hm_5)\sin Vm| = 2Rm|x_{5z}\cos Vm|. \tag{15}$$

Higher sensitivity is obtained for both terms near the pole or on the floor and farther away from the scanner.

*Volumetric length tests*: A symmetrical vertical length test (scanner placed centrally with respect to both ends) is a sensitive position for $x_{5n}$. The symmetrical left and right diagonals are sensitive tests for $x_{5z}$. A symmetrical horizontal length test (scanner placed centrally with respect to both ends) with the length positioned at an elevation (not at scanner height) is sensitive to both $x_{5n}$ and $x_{5z}$.

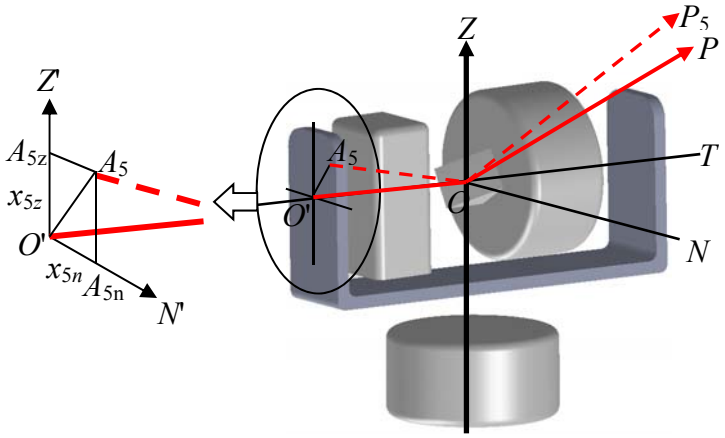


**Figure 5** *Geometry of beam tilt*

### 3.6 Mirror tilt ($x_6$)

*Description*: The plane of the mirror is oriented so that the reflected beam is orthogonal to the incident beam. If the mirror has a small negative tilt $x_6$ (expressed in units of angle) as shown in Fig. 6, the reflected beam is directed towards $P_6$ instead of $P$. This results in the measured horizontal angle being larger than the true angle by $x_6/\sin Vm$. The correction is therefore given by

$$\Delta Hm_6 = 2x_6/\sin Vm. \tag{16}$$

*Two-face tests*: Mirror tilt is sensitive to two-face testing along the horizontal angle direction. The two-face error $E$ is given by

$$E = 2|(\Delta Hm_6)Rm\sin Vm| = 4|x_6 Rm|. \tag{17}$$

The error is larger farther away from the scanner.

*Volumetric length tests*: This term is similar to the well-known collimation error [9] in theodolites and beam tilt in certain types of laser trackers. An asymmetrical diagonal length test is sensitive to this term, as described in [8].

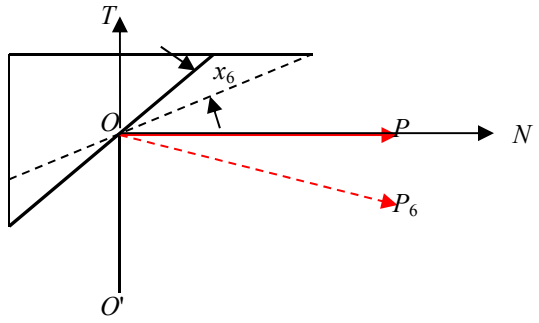


**Figure 6** *Mirror tilt; shown with Vm = 90 degrees*

### 3.7 Transit tilt ($x_7$)

*Description*: The horizontal (transit) and vertical (standing) axes, although intersecting may be non-orthogonal. This lack of squareness between the axes is referred to as transit tilt and is also a common theodolite error source. Again, as in beam and mirror tilt, the parameter $x_7$ is a ratio of offset per unit length and is expressed in units of angle. Lack of squareness between the two axes produces an error only in the measured horizontal angle. Let, $N'$, $T'$, $Z'$ be the coordinate system of the actual scanner, i.e., $T'$ is the actual rotation axis of the mirror; this system is coincident with the $N$, $T$, $Z$ system for the case of a perfect scanner. For an out-of-squareness condition with the $N'$, $T'$, $Z'$ system rotated about the $T$ axis, the result is equivalent to a vertical index offset error (section 3.4) and hence will not be considered further. For an out-of-squareness condition with the $N'$, $T'$, $Z'$ rotated about the $N$ axis (in the right hand sense) by an amount $x_7$, and hence making an angle of $x_7$ between $Z'$ and $Z$) the correction is given by

$$\Delta Hm_7 = -x_7/\tan Vm. \qquad (18)$$

*Two-face tests*: Transit tilt is sensitive to two-face testing along the horizontal angle direction. The error $E$ is given by

$$E = |2(\Delta Hm_7)Rm\sin Vm| = 2Rm|x_7\cos Vm|. \qquad (19)$$

The error is larger near the pole and on the floor and farther away from the scanner.

*Volumetric length tests*: This term is very similar to squareness error in Cartesian CMMs and a symmetrical diagonal length test is sensitive to this error.

### 3.8 Encoder eccentricity ($x_8$ and $x_9$)

*Description*: The horizontal and vertical angle encoder eccentricities contribute to error in the measured angles. The horizontal angle encoder eccentricity can be resolved along the $X$ and $Y$ axes, i.e., ($x_{8x}$, $x_{8y}$) where the coordinates are the center of the encoder wheel in the $X$, $Y$ system, and similarly for the vertical angle encoder eccentricity along $N$ and $Z$ axes, i.e., ($x_{9n}$, $x_{9z}$). The error components $x_8$ and $x_9$ are taken as dimensionless quantities; they are the ratio of the encoder offset to the encoder wheel radius. The corrections are:

$$\Delta Hm_8 = -x_{8x}\sin Hm \qquad (20)$$
$$\Delta Hm_9 = x_{8y}\cos Hm$$

$$\Delta Vm_7 = x_{9n}\cos Vm$$
$$\Delta Vm_8 = -x_{9z}\sin Vm.$$

*Two-face tests*: The term $x_{9z}$ is not sensitive to two-face testing and therefore $\Delta Vm_8$ does not reverse in sign in the back-face. The other terms are sensitive to two-face testing and therefore $\Delta Hm_8$, $\Delta Hm_9$, and $\Delta Vm_7$ do reverse in sign in the back-face. The error $E$ for each of the terms is given by $2|x_{8x}\sin Hm|$, $2|x_{8y}\cos Hm|$, and $2|x_{9n}\cos Vm|$.

*Volumetric length tests*: A symmetrical horizontal length test is sensitive to both the horizontal angle encoder eccentricity terms, $x_{8x}$ and $x_{8y}$. A symmetrical vertical length test is sensitive to $x_{9n}$. A symmetrical horizontal length test (scanner placed centrally with respect to both ends) with the length positioned at an elevation (not at scanner height) is sensitive to $x_{9z}$.

### 3.9 Zero-offset ($x_{10}$)

*Description*: The correction due to the constant error in range is given by

$$\Delta Rm_3 = x_{10}. \quad (21)$$

*Two-face tests*: This term is not sensitive to two-face testing.

*Volumetric length tests*: The zero-offset is sensitive to a length test where the scanner is placed both in-line and in-between two targets (at scanner height), where the distance between targets has already been calibrated by other means.

### 3.10 Second order scale error in the encoder ($x_{11}$ and $x_{12}$)

*Description*: The corrections due to the second order scale error [10] in the encoders are given by

$$\Delta Hm_{10} = x_{11a}\cos 2Hm \quad (22)$$
$$\Delta Hm_{11} = x_{11b}\sin 2Hm$$
$$\Delta Vm_9 = x_{12a}\cos 2Vm$$
$$\Delta Vm_{10} = x_{12b}\sin 2Vm.$$

*Two-face tests*: These terms are not sensitive to two-face testing.

*Volumetric length tests*: Sensitive tests for the horizontal angle scale error have been reported in [10]. These tests involve measuring a symmetrical long horizontal length placed far away from the scanner. Similar special tests for the vertical angle encoder such as a symmetrical long vertical length placed far away can also be envisioned but they will be much more challenging to perform. But tests already described earlier such as the asymmetrical diagonal test and the symmetrical vertical length test are reasonably sensitive to $x_{12a}$ and $x_{12b}$, respectively.

### 3.11Wobble

It is known that laser scanner heads suffer from wobble [11] as they rotate about the vertical axis. We have not yet estimated the magnitude of this problem and therefore do not present any terms in our model to account for this.

## 4 Geometric error model

Combining the corrections $\Delta Hm_i$, $\Delta Vm_i$, and $\Delta Rm_i$, the error model for the scanner is given by

$$\Delta Rm = \Delta Rm_1 + \Delta Rm_3 \tag{23}$$
$$\Delta Hm = \sum_{i=1}^{11} \Delta Hm_i$$
$$\Delta Vm = \sum_{i=1}^{10} \Delta Vm_i \ .$$

Substituting for the terms, we get,

$$\Delta Rm = k(x_2 \sin Vm) + x_{10} \tag{24}$$

$$\Delta Hm = k\left[\frac{x_{1z}}{Rm \tan Vm} + \frac{x_3}{Rm \sin Vm} + \frac{x_{5z}}{\tan Vm} + \frac{2x_6}{\sin Vm} - \frac{x_7}{\tan Vm} - x_{8x} \sin Hm + x_{8y} \cos Hm\right] +$$
$$\left[\frac{x_{1n}}{Rm} + x_{5n} + x_{11a} \cos 2Hm + x_{11b} \sin 2Hm\right]$$

$$\Delta Vm = k\left[\frac{x_{1n} \cos Vm}{Rm} + \frac{x_2 \cos Vm}{Rm} + x_4 \ + x_{5n} \cos Vm + \mathrm{x}_{9n} \cos Vm\right] +$$
$$\left[-\frac{x_{1z} \sin Vm}{Rm} - x_{5z} \sin Vm - \ x_{9z} \sin Vm + x_{12a} \cos 2Vm + x_{12b} \sin 2Vm\right]$$

where $k$ is +1 for the front-face and -1 for the back-face.

The model above shows the corrections due to the different terms for front face measurements ($Vm$ lies between 0 and 180) when $k$ = 1. In order to determine the corrections to the measured coordinates in the back face, the value of $k$ is set to -1, but the vertical angle to be used in the model is still the corresponding front face value, i.e, $Vm$ lies between 0 and 180. In other words, the model assumes that the scanner always reports front face coordinates ($Vm$ lies between 0 and 180). In order to determine the parameters of the model and also to assess the validity of the model itself, we perform a series of experiments using contrast targets. These are described next.

## 5 Contrast targets

The commercially available contrast target is a plate with a partial sphere on the back. On the front-face of the plate is a square that is partitioned into 4 triangles by its two diagonals. Two opposing triangles are black and the other two are white. The point of intersection of the two diagonals on the front-face of the plate is also the theoretical center of the partial sphere. Figs. 7(a) and (b) show views from the front and back of a contrast target, respectively.

The one standard deviation repeatability from 10 consecutive scans in determining the center of three different types of targets as a function of range is shown in Table. 2. The targets include the planar contrast targets and two spherical targets: a 2.375″ diameter ‘Scan Sphere’ and a 4″ Titanium sphere. A software tool provided by the manufacturer of the scanner was used to locate the center of the contrast target while the spherical targets are evaluated for their center location using a custom written least squares sphere fitting algorithm. A point density of 40 points per degree and 40 lines per degree was used in the measurements throughout.

Table 2 indicates that the one standard deviation repeatability in determining the coordinate of a contrast target located 4 m away is generally smaller than 30 μm. This is notably better than the repeatability of determining the center of matte finish spherical targets, which have at least a 40 μm standard deviation. By averaging measurements from 4 scans on contrast targets, we reduce the repeatability of the mean to less than 15 μm. All target coordinate measurements described in subsequent sections are therefore the average from 4 scans.

**Table 2: Repeatability (one standard deviation) in locating target center from 10 consecutive scans as a function of range in units of millimeters**[1]

| | Contrast target | | | Scan sphere | | | Titanium sphere | | |
|---|---|---|---|---|---|---|---|---|---|
| Range | $\sigma_R$ | $R\sigma_H$ | $R\sigma_V$ | $\sigma_R$ | $R\sigma_H$ | $R\sigma_V$ | $\sigma_R$ | $R\sigma_H$ | $R\sigma_V$ |
| 2 m | 0.005 | 0.012 | 0.022 | 0.010 | 0.026 | 0.025 | 0.009 | 0.025 | 0.023 |
| 4 m | 0.005 | 0.019 | 0.033 | 0.017 | 0.024 | 0.042 | 0.020 | 0.024 | 0.042 |
| 6 m | 0.004 | 0.036 | 0.048 | 0.020 | 0.034 | 0.057 | 0.043 | 0.039 | 0.056 |
| 8 m | 0.012 | 0.045 | 0.086 | 0.058 | 0.089 | 0.112 | 0.047 | 0.108 | 0.114 |

1. The terms $\sigma_R$, $\sigma_H$, and $\sigma_V$ refer to the one standard deviation repeatability along the ranging direction (in units of millimeters), the horizontal angle direction (in units of radians), and the vertical angle direction (in units of radians) respectively. In order to compare the repeatability along the range and the angular axes, we scale the one standard deviation repeatability along the angular axes by the nominal range to express them in units of length, hence the notation $R\sigma_H$ and $R\sigma_V$.

We note that contrast targets are not dimensional targets because the coordinate of the center is determined from intensity measurements on the triangles on the front-face of the target. We choose contrast targets for this study as they offer higher repeatability and are therefore more suitable in discerning systematic errors in the instrument under test. Contrast targets also offer a planar surface as opposed to spheres, where the curvature of the surface might produce systematic errors in the determination of the center. But we do understand that contrast targets may not be applicable to all types of large volume scanners.

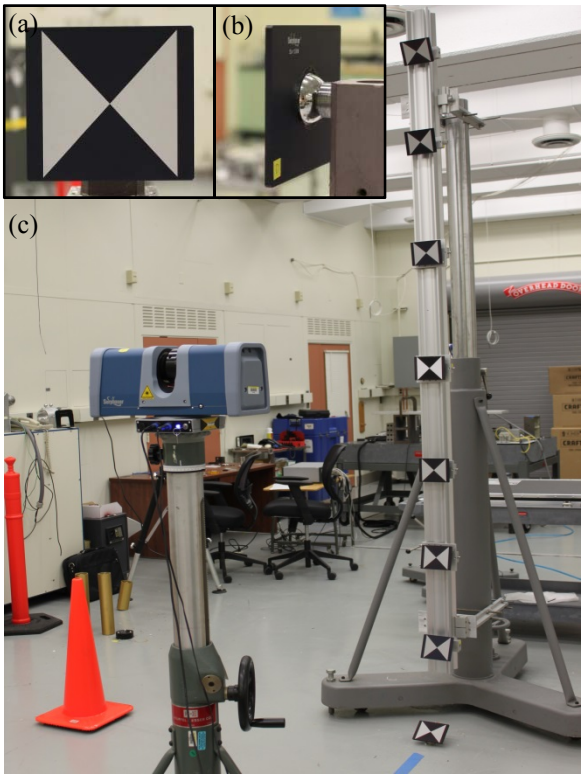


**Figure 7** (a) *View from the front of a contrast target* (b) *view from the back of a contrast target (c) eight contrast targets on a vertical rail for two-face testing*

## 6 Parameter estimation overview

The experiments performed to estimate parameters and establish the effectiveness of the model include a two-face range test, an in-line length test, two-face transverse tests, volumetric length tests using an uncalibrated 8 m length, and volumetric length tests using a calibrated 2.3 m length. We next present a brief overview of the procedure adopted to estimate the parameters and describe key results in subsequent sections.

*Two-face range test:* We first estimate the transit offset $x_2$ by performing front-face and back-face measurements on a target located at scanner height, placed about 2 m from the scanner and examine the difference in the measured range. Half the difference in the change in the range measurements is the transit offset $x_2$. It was determined to be only 0.005 mm for the scanner under test.

*In-line length test*: We then estimate the zero-offset error $x_{10}$ from the in-line length test. For this purpose, we place two nests (at scanner height) that are approximately 4 m apart and calibrate the inter-nest distance using a laser tracker. The scanner is placed centrally, i.e., in-line, between the nests; the alignment is not critical and is performed to the extent the operator can do by visual inspection. The targets are mounted on the nests and scanned in the front-face. While this test is sensitive to both the zero-offset and the transit offset errors, we have already determined the transit offset to be extremely small and hence we can assign the error from the in-line test as twice the zero-offset. The zero-offset was determined to be 0.1 mm in this case.

*Two-face transverse tests*: Two-face transverse tests involve measuring a target in the front-face and then measuring the target again in the back-face and examining the difference in the target coordinates due to systematic errors in the horizontal and vertical angle measurements. These differences can then be fit to the model in section 4 using the method of least-squares. We estimate three parameters, $x_{1n}$, $x_4$, and $x_{5n}$ from the differences between the front- and back-face vertical angle on eight targets located on a vertical rail (we describe the two-face measurements in the next section). We estimate five parameters, $x_{1z}$, $x_3$, $x_6$, $x_{8x}$, and $x_{8y}$, from the differences between the front- and back-face horizontal angles on the same set of eight targets. We also estimate the sum of $x_{5z}$ and $x_7$ from the differences between the front- and back-face horizontal angles and later use volumetric length test results to separate the two quantities. The two-face test procedure and results are described in section 7.

*Volumetric length tests using an 8 m uncalibrated length*: We estimate parameters $x_{11a}$ and $x_{11b}$ associated with second order scale error in the horizontal angle encoder from measurements made on an uncalibrated 8 m long horizontal length. The test procedure and results are described in section 8.

*Volumetric length tests using a 2.3 m calibrated length*: We perform a series of volumetric length tests on a calibrated 2.3 m length and use this data to separate the individual contributions of $x_{5z}$ and $x_7$. The volumetric length tests are described in section 9.

Finally, we note that the beam tilt parameter $x_{9n}$ is indistinguishable from $x_{5n}$ as far as its influence on vertical angle is concerned. We therefore consider $x_{9n}$ to be zero. The term $x_{9z}$ is indistinguishable from $x_{5z}$ and is therefore also considered to be zero. It may be possible to design special volumetric length tests to isolate these terms, but we have not done so at this time. We have also not performed sensitive volumetric length tests to determine the value of the second order scale errors in the vertical angle encoder and therefore we set $x_{12a}$ and $x_{12b}$ to zero.

## 7 Two-face transverse tests using contrast targets on a vertical rail

We placed 8 contrast targets on a vertical rail as shown in Fig. 7(c). The laser scanner was first placed about 2 m away (we refer to this as the near position) from the rail and it was raised so that the target on the floor is just visible in the field of view. We performed 4 scans and determined the average front- and back-face coordinate of each target. We then rotated the laser scanner and stand by 45º and again performed 4 scans. The rotation of the stand is a coarse operation; any tilt and translations in the stand are not of any consequence as the purpose of this experiment is to document the two-face errors of the different targets from various positions and orientations of the scanner.

In this manner, we acquired front-face and back-face coordinates for each of the 8 targets at each of the 9 clocking angles (horizontal angles) of the stand: 0º, 45º, 90º, 135º, 180º, 225º, 270º, 315º, 360º. The last clocking angle is a duplicate of the first position to determine if there are any closure errors. We then moved the laser scanner to a distance of about 4 m away from the rail (we refer to this as the far position). We repeated the same sequence of measurements as described earlier. For each of the 9 clocking angles of the laser scanner, we determined the average front-face and back-face coordinate of each target based on 4 scans.

For the 8 targets and 9 clocking angles at the near scanner position, there are 72 front-face coordinates and 72 back-face coordinates. We calculate the difference, *dHm*, between the front- and back-face horizontal angles for the 9 clocking angles at the near scanner position and plot that in Fig. 8(a). We calculate the difference, *dHm*, between the front- and back-face horizontal angles for the 9 clocking angles at the far scanner position and plot that in Fig. 8(b). Figs. 8(a) and (b) also show the results of the model prediction for the two cases.

There are two important points to note in the data in Figs. 8(a) and (b). First is the systematic error or trend seen from targets 1 through 8 for any given clocking position. The second is the negative bias in those errors. The model predicts that the transit tilt $x_7$ is the primary contributor to the trend in the errors while mirror tilt $x_6$ is the source of the bias. In section 9, we will show volumetric length test results that confirm the presence of transit tilt in our scanner. The mirror tilt does not manifest in the volumetric length test as it is not of sufficiently large magnitude.

Similar front- and back-face differences, *dVm*, along with model predictions are shown for the vertical angle, for the near and far position in Figs. 8(c) and 8(d). Again, we note the trend in the errors at any given clocking angle along with the negative bias in the errors. The model predicts that the trend in the errors is due to beam tilt $x_{5n}$, while the bias is due to vertical index offset $x_4$. In section 9, we will show volumetric length test results that confirm the presence of beam tilt in our scanner. The vertical index offset, however, was not large enough to influence the volumetric length tests that we performed.

Fig. 8 indicates that the largest front-face to back-face difference was about 200 μrad for both the horizontal and vertical angle for a target that is about 4 m away. This translates to a linear error of 0.8 mm front-face to back-face difference. In other words, if the scanner were used to measure this target in front-face alone (or in back-face alone), the error in locating the target would be about 0.4 mm.

The model predictions are shown in Fig. 8 as blue lines. The model does an excellent job of fitting to the data; the residual errors are generally on the order of 20 μrad. This, then, implies that at a 4 m distance, an error of 0.4 mm would be reduced to 0.04 mm after error correction using the model, which is a ten-fold improvement in accuracy. The measurements shown in Fig. 8 were repeated over a period of several months and the results were found to be stable. Clearly, stability is important for purposes of compensation.

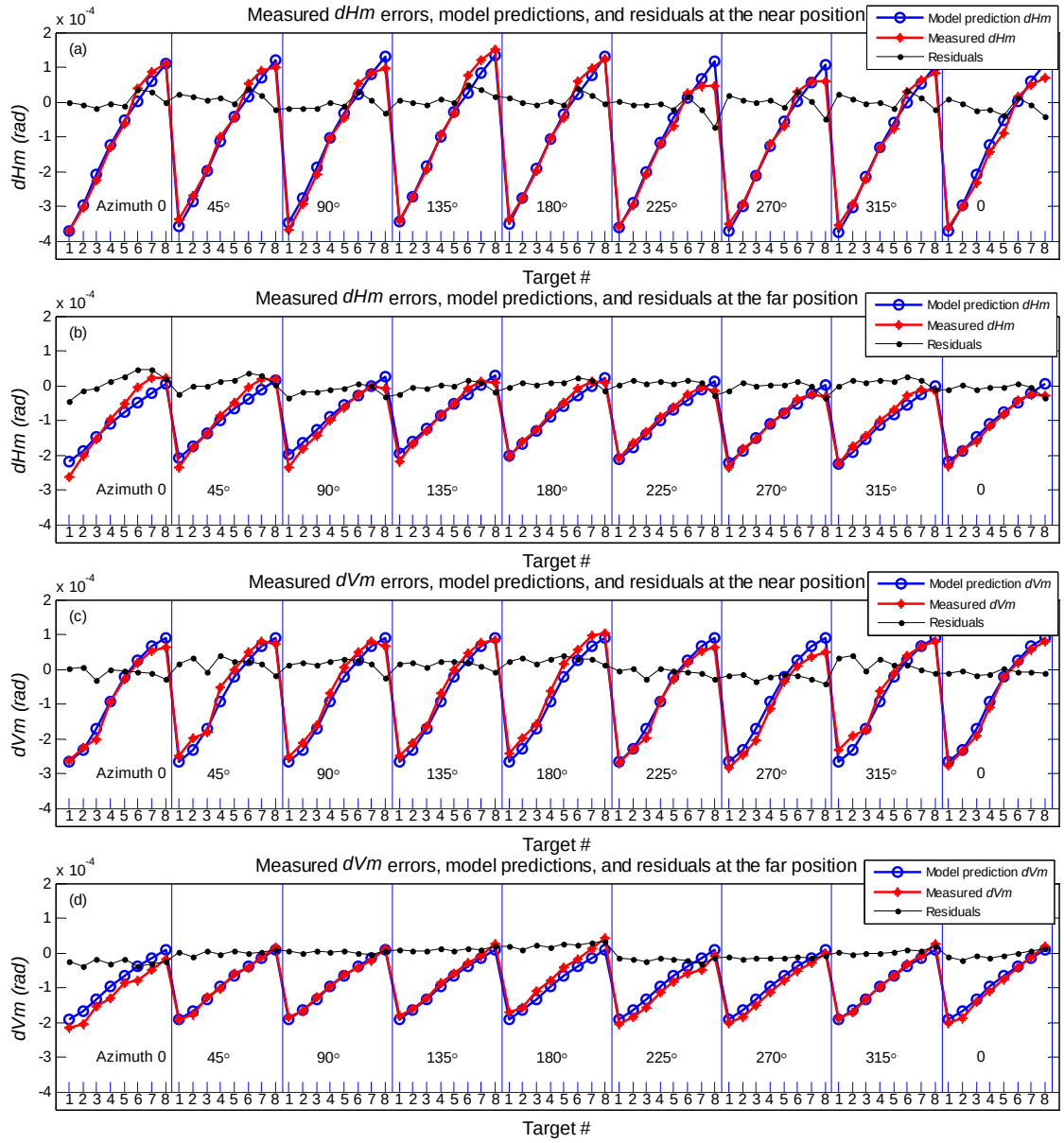


**Figure 8** (a) *Measured difference between front- and back-face horizontal angle for the 9 clocking angles at the near position (2* m*) along with model predictions* (b) *Measured difference between front- and back-face horizontal angle for the 9 clocking angles at the far position (4* m*) along with model predictions* (c) *Measured difference between front- and back-face vertical angle for the 9 clocking angles at the near position (2* m*) along with model predictions* (d) *Measured difference between front- and back-face vertical angle for the 9 clocking angles at the far position (4* m*) along with model predictions*

Note that we use the notation *dHm* and *dVm* to denote the difference between front- and back-face angles (measured or model predictions), and $\Delta Hm$ and $\Delta Vm$ to denote the model based corrections to the measured angles *Hm* and *Vm*. For a term that is sensitive to two-face testing, the magnitude of the front-face to back-face difference *dHm* (*dVm)* will be twice the correction $\Delta Hm$ ($\Delta Vm$) because the corrections reverse in sign in the back-face.

## 8 Volumetric length tests using an 8 m uncalibrated length

We placed two contrast targets on stands that were approximately 8 m apart and at scanner height. The scanner itself was placed centrally with respect to the nests and about 8 m away from the horizontal length created by the two nests. We measured the length between the two targets from 20 different azimuth positions (clocking angles) of the scanner in its front-face. The resulting lengths are shown as a function of the azimuth in Fig. 9, where a clear second order sinusoidal error is discernible. We estimate the two parameters $x_{11a}$ and $x_{11b}$ from these tests using the procedure described in [10]. The values for these parameters were determined to be 22 µrad and 19 µrad respectively. The model predictions based on the computed parameters are also shown in the figure. The model does an excellent job of fitting to the data with the residual errors being smaller than ±0.1 mm.

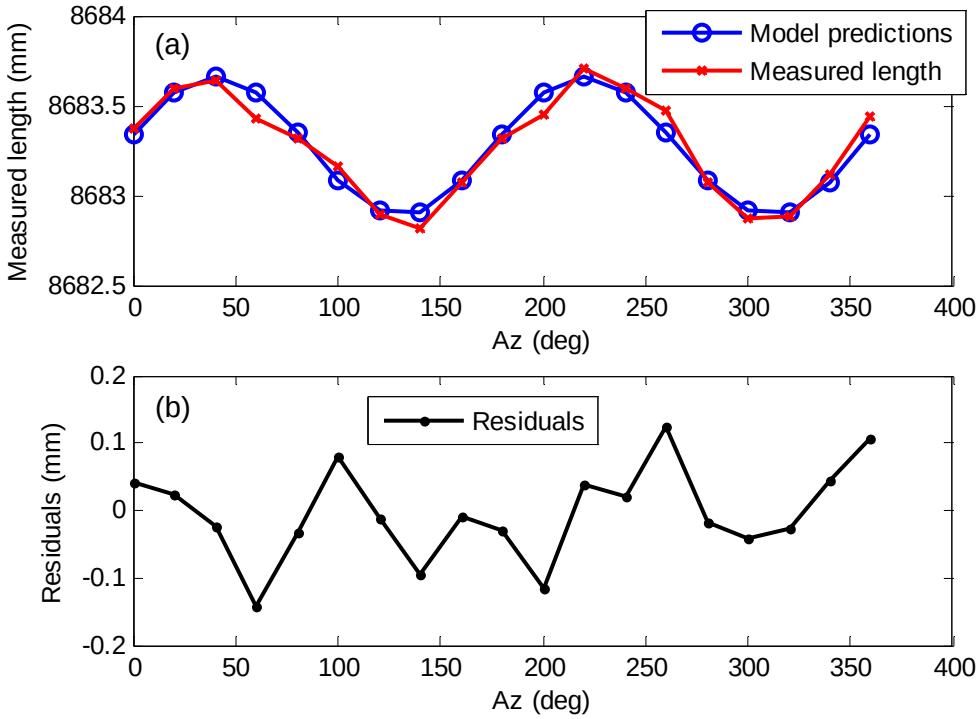


**Figure 9** (a) *Results from the second order scale error test showing measured length and model predictions as a function of azimuth* (b) *Residuals from the second order test*

## 9 Volumetric length tests using a 2.3 m calibrated length

A 2.3 m long scale bar is mounted on a rotary table in our laboratory, see Fig. 10. The center-to-center distance of this scale bar is calibrated using a laser tracker and 1.5″ spherically mounted retro-reflectors that seat into kinematic nests on the bar. The expanded uncertainty in the length is 0.01 mm ($k$ = 2). After calibration, we place a contrast target into the nests at each end of the scale bar. The center-to-center length of this scale bar is measured by the scanner from different positions. The scale bar is also rotated to the horizontal, vertical, and diagonal orientations. A total of 9 scanner/scale bar positions/orientations were considered. For each of those 9 positions/orientations, 4 clocking angles of the scanner were considered. A total of 36 lengths were therefore measured. At any given position/orientation, we perform four scans and consider

the average as the measured length. The results are shown in Fig. 11 and are used to determine parameters $x_{5z}$ and $x_7$ through a least squares fit of the data.

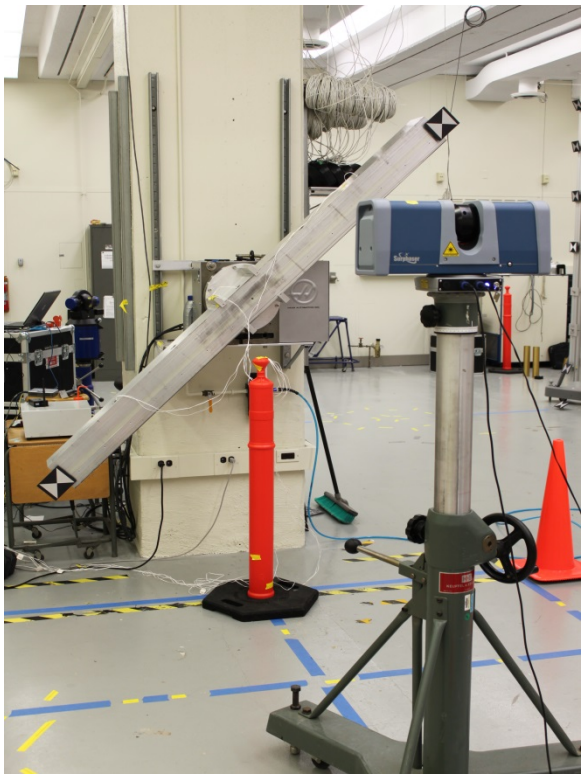

**Figure 10** *Volumetric length testing of position 5 (symmetrical right diagonal) shown.*

The 9 positions/orientations of the scanner/scale bar considered are described below:

Position 1 – symmetrical horizontal length test: The scale bar is horizontal with the scanner placed centrally and about 1 m from the bar. The scanner is at the same height as the bar.

Position 2 - symmetrical horizontal length test: The scale bar is horizontal with the scanner placed centrally and about 3 m from the bar. The scanner is at the same height as the bar.

Position 3 - symmetrical vertical length test: The scale bar is vertical with the scanner placed centrally and about 1 m from the bar. The scanner is raised so that the head is at the same height as the bar center.

Position 4 - symmetrical left diagonal length test: The scale bar is diagonal (left side is high, right side is low) with the scanner placed centrally and about 1 m from the bar. The scanner head is at the same height as the bar center.

Position 5 - symmetrical right diagonal length test: The scale bar is diagonal (right side is high, left side is low) with the scanner placed centrally and about 1 m from the bar. The scanner head is at the same height as the bar center.

Position 6 – asymmetrical horizontal length test, left: The scale bar is horizontal with the scanner placed near the left end of the bar and about 1 m from the bar. The scanner is at the same height as the bar.

Position 7 – asymmetrical horizontal length test, right: The scale bar is horizontal with the scanner placed near the right end of the bar and about 1 m from the bar. The scanner is at the same height as the bar.
Position 8 – asymmetrical diagonal length test 1: The scale bar is in the left diagonal position (left side raised, right side low). The scanner is placed near the right target, but raised so that it is at the same height as the left target.
Position 9 – asymmetrical diagonal length test 2: The scale bar is in the right diagonal position (right side raised, left side low). The scanner is placed near the left target, but raised so that it is at the same height as the right target

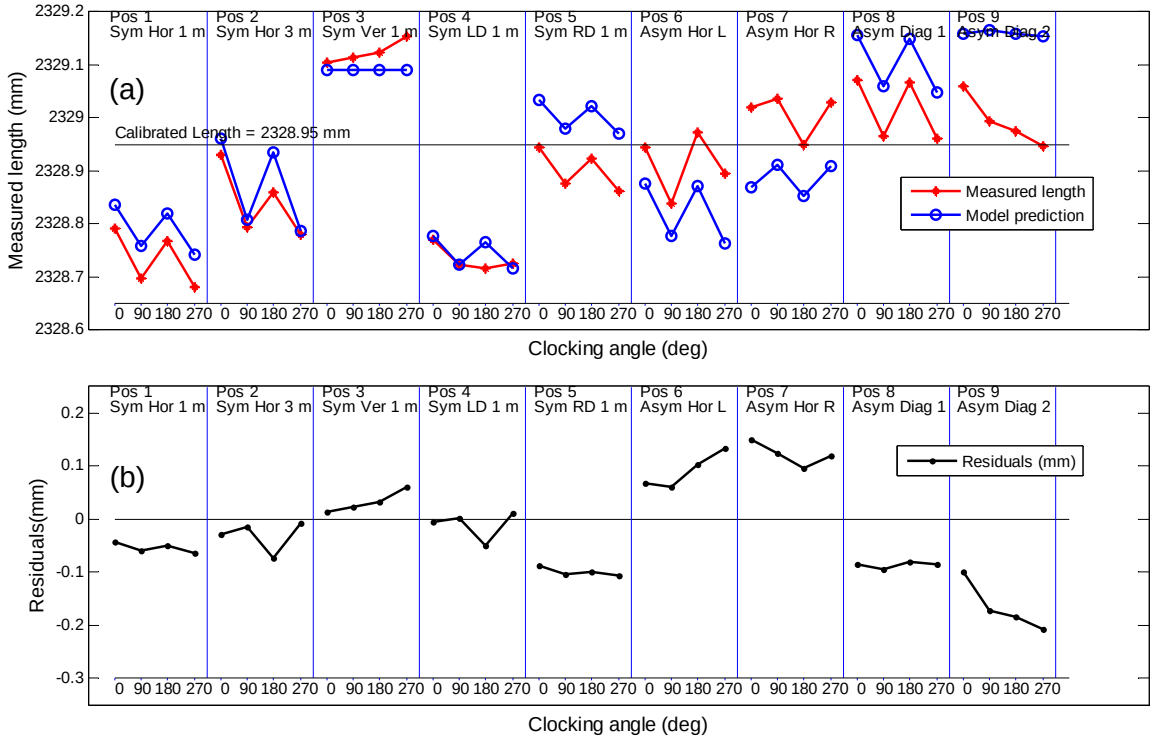


**Figure 11** (a) *Measured lengths and model predictions for the 36 positions/orientations* (b) *Residuals for the 36 positions/orientations.*

The model does a resonable job of predicting measured errors for the 9 different positions/orientations of the scanner/scale bar with residuals generally on the order of about 0.1 mm. There are three points worth emphasizing.

First, we note that Fig. 11 shows approximately 200 µm difference in length between the left (position 4) and right (position 5) symmetrical diagonal length tests. This is an indication of squareness (transit tilt) problem in the system. These data are thus a validation of a model prediction made earlier, in which the trend in the horizontal angle two-face measurements was indicative of transit tilt.

Second, we note that Fig. 11 shows that the symmetrical vertical length test (position 3) has a positive bias, whereas most other length errors are negatively biased. Our model suggests that this is an indication of beam tilt in the system. Again, the results in Fig. 11 are a validation of a

model prediction made earlier, in which the trend in the vertical angle two-face measurements was indicative of beam tilt.

Finally, we note that there exists a saw-tooth pattern in the measured length from the four clocking positions at any given position. Our model suggests that this is an indication of second order scale error in the horizontal angle encoder. In fact, model predictions clearly capture the saw-tooth pattern seen in the measurement data. These length tests thus reinforce earlier results obtained from an uncalibrated 8 m length, which suggested the presence of a second order scale error in the horizontal angle encoder.

While the model does a reasonable job of predicting most of the errors, we observe an offset between the measured length and the model. This is sometimes as large as 0.2 mm, as seen for position 9, in Fig. 11. Target properties such as eccentricity in construction, tilt (angle of incidence), etc, influence measurement results. We are currently working to reduce this source of error so that we can perform length measurements with higher accuracy. It should be noted that target-induced errors are common-mode in two-face testing, but not in volumetric length tests.

## 10 Model parameters and dominant terms

For purpose of completeness, we present the model parameters determined from the data in Table 3.

**Table 3: Model parameters for the scanner**

| Parameter | Description | Value |
|---|---|---|
| $x_{1n}$ | Beam offset along *n* | 0.024 mm |
| $x_{1z}$ | Beam offset along *z* | 0.015 mm |
| $x_2$ | Transit offset | 0.005 mm |
| $x_3$ | Mirror offset | 0.033 mm |
| $x_4$ | Vertical index offset | 0.000049 rad |
| $x_{5n}$ | Beam tilt along *n* | 0.000123 rad |
| $x_{5z}$ | Beam tilt along *z* | 0.000034 rad |
| $x_6$ | Mirror tilt | 0.000021 rad |
| $x_7$ | Transit tilt | -0.0001 rad |
| $x_{8x}$ | Horizontal angle encoder eccentricity along *x* | 0.000005 |
| $x_{8y}$ | Horizontal angle encoder eccentricity along *y* | -0.000006 |
| $x_{9n}$ | Vertical angle encoder eccentricity along *n* | Not determined |
| $x_{9z}$ | Vertical angle encoder eccentricity along *z* | Not determined |
| $x_{10}$ | Bird-bath error | 0.1 mm |
| $x_{11a}$ | Second order scale error in the horizontal angle encoder | 0.000022 rad |
| $x_{11b}$ | Second order scale error in the horizontal angle encoder | 0.000019 rad |
| $x_{12a}$ | Second order scale error in the vertical angle encoder | Not determined |
| $x_{12b}$ | Second order scale error in the vertical angle encoder | Not determined |

In Fig. 12, we plot the relative contributions of each of the model terms separately to the *dHm* and *dVm* errors (two-face errors) for the eight targets on the vertical rail. We show the results only for the first clocking angle (horizontal angle of zero) and at the near position. The plot is informative in that it clearly captures the leading contributor for the observed two-face errors in the horizontal angle as the transit tilt ($x_7$) and the leading contributor for the observed vertical angle two-face errors as the beam tilt along the *ON* ($x_{5n}$) axis. Fig. 12 also suggests that the leading contributor to the negative bias in the horizontal angle two-face errors is the mirror tilt, $x_6$ and that the leading contributor to the negative bias in the vertical angle two-face errors is the vertical index offset, $x_4$.

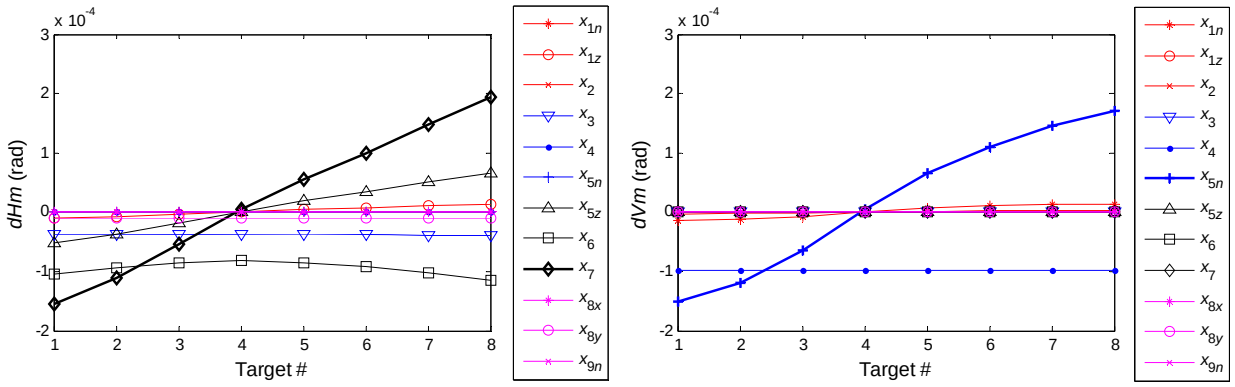


**Figure 12** *Relative contributions of the different model terms to differences between front-face and back-face errors dHm and dVm. The contribution from some terms are not shown here as they are not sensitive to two-face testing.*

## 11 Conclusions and future work

We describe a geometric error model for a large volume laser scanner that has a spinning prism mirror mounted on the gimbal head to direct the laser to the target. We determine the model parameters and demonstrate its effectiveness by performing several two-face and volumetric length experiments. We show that measured two-face errors are on the order of 200 µrad at 4 m (which translates to 800 µm at 4 m) for the scanner we tested, which is much larger than the repeatability in locating the target. Further, the residuals from our fit are on the order of 20 µrad, thus suggesting that our model can in fact be applied to improve the accuracy of the instrument. Geometric error models are important not only in improving the accuracy of the instrument but also in understanding error sources and developing standardized test procedures that are sensitive to all known sources of error. In this paper, we therefore not only document the different misalignment terms but also describe their influence on measured range and angles. We then suggest target placement for two-face and length tests to achieve high sensitivity to the different terms. This work therefore lays the foundation for possible future work in the area of laser scanner volumetric performance evaluation and documentary standards development.

**Disclaimer:** Commercial equipment and materials may be identified in order to adequately specify certain procedures. In no case does such identification imply recommendation or endorsement by the National Institute of Standards and Technology, nor does it imply that the materials or equipment identified are necessarily the best available for the purpose.

## References

1. Raimund Loser, Stephen Kyle, Alignment and field check procedures for the Leica Laser Tracker LTD 500, Boeing Large Scale Optical Metrology Seminar, 1999
2. United States Patent number US 7,973,912 B2, Binary modulation rangefinder, Peter Petrov, Yuri Yakovlev, Vladimir Grigorievsky, Andrey Astrelin, Alex Sherstuk, July 5, 2011
3. Derek D.Lichti, A review of geometric models and self-calibration methods for terrestrial laser scanners, Boletim de Ciencias Geodesicas, Volume 16, Issue 1, 2010, Pages 3-19
4. Derek D.Lichti, Terrestrial laser scanner self-calibration: Correlation sources and their mitigation, ISPRS Journal of Photogrammetry and Remote Sensing 65 (2010) 93-102

5. D. García-San-Miguel, J.L. Lerma, Geometric calibration of a terrestrial laser scanner with local additional parameters: An automatic strategy, ISPRS Journal of Photogrammetry and Remote Sensing, Volume 79, May 2013, Pages 122–136
6. Derek D.Lichti, Error modelling, calibration and analysis of an AM–CW terrestrial laser scanner system, ISPRS Journal of Photogrammetry and Remote Sensing, 61 (5), January 2007, 307-324
7. ASME B89.4.19-2006 Standard - *Performance Evaluation of Laser-Based Spherical Coordinate Measurement Systems*, www.asme.org.
8. B. Muralikrishnan, D. Sawyer, C. Blackburn, S. Phillips, B. Borchardt, W. T. Estler, ASME B89.4.19 performance evaluation tests and geometric errors in laser trackers, NIST Journal of Research, 114 (1), p. 21-35, 2009
9. Fritz Deumlich, Surveying Instruments, Walter de Gruyter, Berlin/New York (1982)
10. B. Muralikrishnan, C. Blackburn, D. Sawyer, S. Phillips, and R. Bridges, Measuring scale errors in a laser tracker's horizontal angle encoder through simple length measurement and two-face system tests, Journal of Research of the NIST, 115 (5), p.291-301, 2010
11. Jacky C.K. Chow, Derek D. Lichti, and William F. Teskey, Accuracy assessment of the faro focus3D and leica HDS6100 panoramic type terrestrial laser scanner through point-based and plane-based user self-calibration. FIG Working Week 2012: *Knowing to manage the territory, protect the environment, evaluate the cultural heritage*. Rome, Italy. May 6-10, 2012.